

# Aluminium structures exposed to fire conditions – an overview

J. Maljaars

TNO Built Environment and Geosciences, Delft, the Netherlands <sup>1</sup>

L. Twilt

Formerly TNO Built Environment and Geosciences, Delft, the Netherlands

J. H. H. Fellingner

Max-Planck-Institut für plasmaphysik, Garching, Germany

H. H. Snijder

Eindhoven University of Technology, Eindhoven, the Netherlands

F. Soetens

Eindhoven University of Technology and TNO Built Environment and Geosciences,  
Delft, the Netherlands

**This paper gives an overview of the structural behaviour and design of aluminium structures exposed to fire conditions. Two design approaches are elaborated: the “traditional” approach that is mainly based on conventions and the fire safety engineering approach that is more based on physics. For the traditional approach, equations for the aluminium member temperature are provided, mechanical properties are given and recently developed calculation models for flexural buckling, local buckling and heat affected zone rupture are presented. For the fire safety engineering approach the possibilities for evaluation of member temperature are provided, a constitutive model for aluminium alloys is given which can be implemented in finite element programmes and two design examples are presented to show the evaluation of the structural behaviour. The paper concludes that the fire safety engineering approach is preferred for the fire resistance evaluation in particular for structures made of materials sensitive to fire conditions, such as aluminium alloys.**

---

<sup>1</sup> email [johan.maljaars@tno.nl](mailto:johan.maljaars@tno.nl), telephone +31 15 2763464

*Keywords: Fire design, fire safety engineering, elevated temperature, heating, creep, aluminium, local buckling, flexural buckling, heat affected zone*

## **1 Introduction**

Aluminium alloys (hereafter called aluminium) are used more and more in load-bearing structures such as bodies of fast ships and yachts, parts of drill platforms and roofs with large spans. The main advantageous material properties in this respect are the relatively high ratio between the strength and the density, the relatively good corrosion resistance and the possibility to extrude sections which provides the possibility to design optimal sections. One of the main drawbacks of aluminium of the above mentioned applications is the relatively fast reduction of constitutive properties at elevated temperatures. This is why fire design is an important part of the entire design for many aluminium structures.

Recently, a number of research studies were undertaken in The Netherlands into the behaviour of fire exposed aluminium structures. A PhD study focussed on the constitutive properties of the material and on the failure mechanism of local buckling of columns [Maljaars, 2008]. A joint-industry project provided design strategies and gave insight into flexural buckling of columns and the behaviour of welded connections [Maljaars and Soetens, 2006 and 2009a]. A second PhD study recently started on the behaviour of beams (Van der Meulen, 2009). This paper gives an overview of the knowledge in [Maljaars, 2008] and [Maljaars and Soetens, 2006 and 2009a]. The paper distinguishes between the two major design strategies used in practice. The “traditional” fire design approach is mainly based on conventions, while the fire safety engineering (FSE) strategy is more based on physical and mechanical principles. In the latter strategy, the fire model and the mechanical response model provide a better approximation of reality as compared to the former strategy. Background to both strategies are provided e.g. in [Dotreppe et al., 1990], [Kruppa, 1996], [Kruppa et al., 2005] and [Twilt et al., 1991]. Table I gives an overview of the different steps that need to be undertaken in these strategies. The first two steps are independent of the structural material and are not elaborated in this paper. This paper focuses on steps 3-5. Note that the FSE approach is suitable for a probabilistic evaluation (level II or level III evaluation) as well as for an evaluation with “fixed” values for parameters in combination with partial factors (level I evaluation). This paper uses a level I evaluation.

## 2 Heating

### 2.1 Relevant thermal material properties

The member temperature is determined on the basis of heat transfer properties, aluminium properties and – if applied – characteristics of the fire insulation. The relevant gas properties - resulting from step 2 of Table 1 - are:

- Gas temperature  $\theta_g$  and convection coefficient  $\alpha_c$ , for heating by convection;
- Radiation temperature  $\theta_r$  and emissivity of the fire  $\varepsilon_{fi}$ , for heating by radiation.

The relevant aluminium properties are:

- Thermal conductivity  $\lambda_{al}$ , The thermal conductivity depends on the temperature and the alloy. At room temperature  $\lambda_{al}$  is between 100 and 250 W/mK, depending on the alloy [Kammer, 2002], [Holman, 2010] and [Gale and Totemeier, 2003]. The values for  $\lambda_{al}$  increase at elevated temperature. The high value for  $\lambda_{al}$  – several times higher than that of steel – in combination with the thin-walled sections used in aluminium structures implies that the aluminium temperature is uniform over the thickness of the aluminium profile.

Table 1: Steps in a “traditional” approach and in a FSE approach

Steps	“traditional” approach	FSE approach (level 1)
1. required fire resistance	According to (inter)national regulations (30 – 120 min.)	Time required for escape and search, or survival of the structure
2. gas temperature	Nominal temperature-time curves (such as the standard curve)	Natural fires, determined with Zone models or CFD models
3. member temperature	Simple calc. model in standards (uniform temperature)	Numerical models (CFD or finite element models)
4. mechanical properties	Values in standards such as [EN 1999-1-2, 2007]	Constitutive models incl. creep, or properties derived from these models
5. structural response	Component approach, using simple calculation rules in standards	Part of the structure or entire structure, using numerical models

- Thermal capacitance, which is the product of specific heat  $c_{al}$  and density  $\rho_{al}$ . Both values vary little between alloys. The specific heat increases from  $c_{al} \approx 900$  J/kg °C at room temperature to  $c_{al} \approx 1100$  J/kg °C at 500 °C [Kammer, 2002]. The density is  $\rho_{al} \approx 2700$  kg/m<sup>3</sup>;
- Emissivity of aluminium  $\epsilon_{al}$ . The value for  $\epsilon_{al}$  depends on the alloy and the thickness of the corrosion layer – related to the age and environment of the structure. The value for  $\epsilon_{al}$  varies from 0.03 to 0.31 [Kammer, 2002], [Holman, 2010] and [Twilt, 1991]. These values apply for unprotected members not engulfed in flames. For members covered with paint, insulation or soot, [EN 1999-1-2, 2007] specifies a generalised value of 0.7.

A number of demands for fire insulation materials can be distinguished when applied on aluminium structures:

- Aluminium loses its strength at temperatures roughly between 200 – 350 °C (Section 3). Thus, the insulation material should be effective at these temperatures. This is of importance e.g. for intumescent materials;
- The low self-weight of the structure is in many cases an important reason for applying aluminium. A low self-weight of the insulation layer is thus beneficial or even required, i.e. the density of the insulation material  $\rho_p$  should be low and/or the thickness of the layer  $d_p$  should be small;
- The above implies that the thermal capacity of the insulation layer is limited so that the insulating property should especially come from a low thermal conductivity  $\lambda_p$  ;
- The insulation material should not cause or promote corrosion of aluminium;
- The insulation material should remain coherent and cohesive to the structural member. This so-called “stickability” on aluminium might be different as compared with application on steel e.g. because of the larger thermal and mechanical deformations to be expected for aluminium (Section 3). The insulation material should be flexible enough to follow these deformations without (severe) cracking. The “stickability” has to be determined in tests;

## 2.2 Member temperature calculation in a “traditional” fire design approach

The fact that the aluminium temperature  $\theta_{al}$  is uniform through thickness – due to the high thermal conductivity – can be used to derive simple equations with which the member

temperature versus time curve is determined. The iterative equations (1) for unprotected aluminium and (2) for protected aluminium are provided by [EN 1999-1-2, 2007] (symbols are explained at the end of the paper):

$$\Delta\theta_{al} = k_{sh} \frac{1}{c_{al} \rho_{al}} \frac{A_m}{V} h_{met} \Delta t \quad (1)$$

$$\Delta\theta_{al} = \max \left( \frac{\lambda_p / d_p}{c_{al} \rho_{al}} \frac{A_p}{V} \left[ \frac{1}{1 + \phi / 3} \right] (\theta_g - \theta_{al}) \Delta t - (e^{\phi / 10} - 1) \Delta\theta_g, 0 \right) \quad (2a)$$

$$\phi = \frac{c_p \rho_p}{c_{al} \rho_{al}} d_p \frac{A_p}{V} \quad (2b)$$

The section factors  $A_m / V$  and  $A_p / V$  are equal to the surface exposed to the fire divided by the volume. In case of a member directly exposed on three sides – e.g. where a beam is in contact with a ceiling slab, cases 2 and 3 in Figure 1 – the smaller exposed surface causes the calculated temperature to be lower than the same member fully engulfed in flames. Using equations (1) and (2), the calculated member temperature is uniform through the cross-section even for members not exposed on all sides (cases (2) and (3) in Figure 1). This is an approximation; the real member temperature at the unexposed side is lower than at the most exposed side. The thermal properties of the fire insulation material  $c_p$  and  $\lambda_p$  usually depend on the temperature. In equation (2) these properties are specified as a function of the aluminium temperature resulting in artificial values for  $\lambda_p$ . These have to be determined in tests. Theoretically the relationships between  $\lambda_p$  and  $\theta_{al}$  are equal as for steel in case of an undamaged insulation layer that remains attached to the member surface. However, the “stickability” on aluminium may be different from steel and the

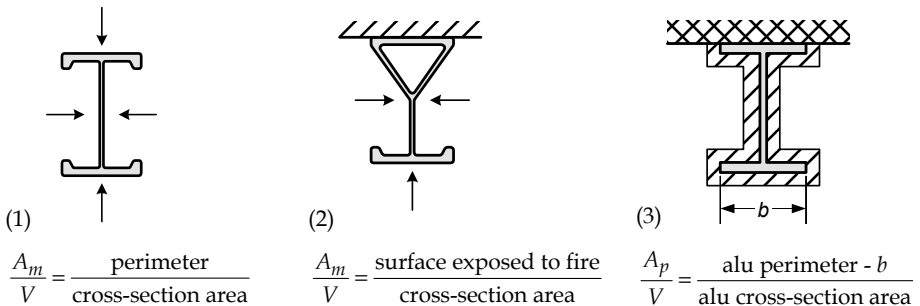


Figure 1: Examples of the definition of the section factor (source: [EN 1999-1-2, 2007])

larger coefficient of thermal expansion and larger creep strain of aluminium may cause that holes or cracks in the insulation layer occur at lower temperatures. Separate tests on aluminium members are required in order to accurately determine the relationship between  $\lambda_p$  and  $\theta_{al}$ . In absence of such tests, the relationship determined in tests on steel members provides a first guess.

### 2.3 Member temperature calculation in a FSE approach

Distinction is made between insulated and non-insulated members, and in members fully engulfed in flames and members exposed at three sides.

- *Non-insulated members engulfed in flames.* Equation (1) can be used for determining the temperature.
- *Non-insulated members exposed at three sides.* As mentioned above, the temperature gradient cannot be determined with equation (1). Whether the approximated uniform temperature according to equation (1) is allowable in a FSE approach depends on the required level of accuracy. The temperature over the cross-section can be determined using finite element (FE) analyses or, when computational fluid dynamics (CFD) is applied for the temperature distribution in the compartment, the member temperature can be determined directly in the CFD model.
- *Insulated members engulfed in flames, with equal insulation at all sides.* Equation (2) is an approximate equation derived for the standard temperature-time curve [Wang and Tan, 2006]. This equation is not applicable for natural fires, especially not in the decay phase of the fire and for heavily insulated members. A conservative result is obtained by neglecting the thermal capacity of the insulation material, i.e.  $\phi = 0$ . Alternatively a FE analysis or a CFD analysis may give more accurate results. Usually a 1-dimensional FE analysis suffices. Note that the thermal conductivity of the insulation material in an FE or CFD analysis is the real conductivity, i.e. specified as a function of the insulation temperature instead of the aluminium temperature. (Examples of) FE or CFD models accounting for cracks and holes in the insulation layer developing during the fire are not found in literature.
- *Insulated members exposed on three sides or with unequal insulation.* A FE or CFD analysis is required in order to obtain the temperature distribution across the member cross-section. Usually a 2-dimensional FE analysis suffices.

### 3 Mechanical properties

Relevant parameters and phenomena that determine the mechanical properties of aluminium alloys at elevated temperature are thermal expansion, elasticity, plasticity and creep (visco-elasticity and visco-plasticity). These phenomena are discussed in this chapter.

#### 3.1 Thermal expansion

Data in [Kammer, 2002] and [Gale and Totemeier, 2003] indicate that the coefficient of linear thermal expansion  $\alpha_\theta$  is almost independent of the alloy. Equation (3) is obtained by curve fitting for  $\alpha_\theta$  between 20 °C and temperature  $\theta_{al}$ .

$$\alpha_\theta = 22.5 \cdot 10^{-6} + 0.01 \cdot 10^6 \cdot \theta_{al} \quad (3)$$

The relative elongation  $\varepsilon_{th} = \Delta L / L$  given in [EN 1999-1-2, 2007] is based on this relationship.

#### 3.2 Elasticity

The modulus of elasticity  $E_\theta = \sigma / \varepsilon_{el,\theta}$  is determined in tensile tests [Kaufman, 1999] and bending tests [Maljaars, 2008]. An overview of the bending test set-up is presented in Figure 2. Bending tests were carried out at several temperatures on specimens of alloy 5083-H111 and alloy 6060-T66. Equations (4) and (5) represent  $E_\theta$  derived from the bending tests. Data in [Kaufman, 1999] indicate that  $E_\theta$  depends on the alloy series, but is almost independent of the alloy type within a series. Equations (4) and (5) are representative for 5xxx and 6xxx series alloys, respectively.

$$\text{Alloys 5xxx:} \quad E_\theta = 72000 - 10 \cdot \theta_{al} - 0.21 \cdot \theta_{al}^2 \quad \text{for } 20 \text{ }^\circ\text{C} \leq \theta_{al} \leq 350 \text{ }^\circ\text{C} \quad (4)$$

$$\text{Alloys 6xxx:} \quad E_\theta = 69000 - 10 \cdot \theta_{al} - 0.21 \cdot \theta_{al}^2 \quad \text{for } 20 \text{ }^\circ\text{C} \leq \theta_{al} \leq 350 \text{ }^\circ\text{C} \quad (5)$$

[EN 1999-1-2, 2007] provides values for the modulus of elasticity at elevated temperatures independent of the alloy series. These values are similar to the relationships by equations (4) and (5) (maximum difference 5 % for temperatures up to 300 °C).

### 3.3 Stress-strain relationships in a “traditional” fire design approach

In most traditional approaches - including the simple calculation models in [EN1999-1-2, 2007] - the stress-strain relationships are represented by bi-linear relationships. The fact that the real relationship is significantly curved (Section 3.5) is taken into account in the design models for the failure mechanisms (Section 4). The yield stress defined in [EN1993-1-2, 2005] for steel is the stress at a plastic strain of 2%  $f_2$ . In [EN 1999-1-2, 2007] for aluminium the yield stress is defined as the stress at a plastic strain of 0.2%  $f_{0,2}$ . Values in the standard for  $f_{0,2}$  are obtained from steady state tensile tests, i.e. tensile tests carried out with a certain strain rate at a constant temperature after a certain period of exposure to this temperature. Figure 3 gives some examples. The legend in this figure indicates the test temperature and - between brackets - the strain rate before the attainment of  $f_{0,2}$  and the strain rate from  $f_{0,2}$  up to rupture. The figure shows that the steady-state stress-strain curve depends on the temperature and on the strain rate (compare results at  $\theta_{fl} = 176$  °C and 178 °C). This strain rate sensitivity is significantly larger than at room temperature. The steady-state stress-strain relationship further depends on the thermal exposure period (shown by data in [Kaufman, 1999]).

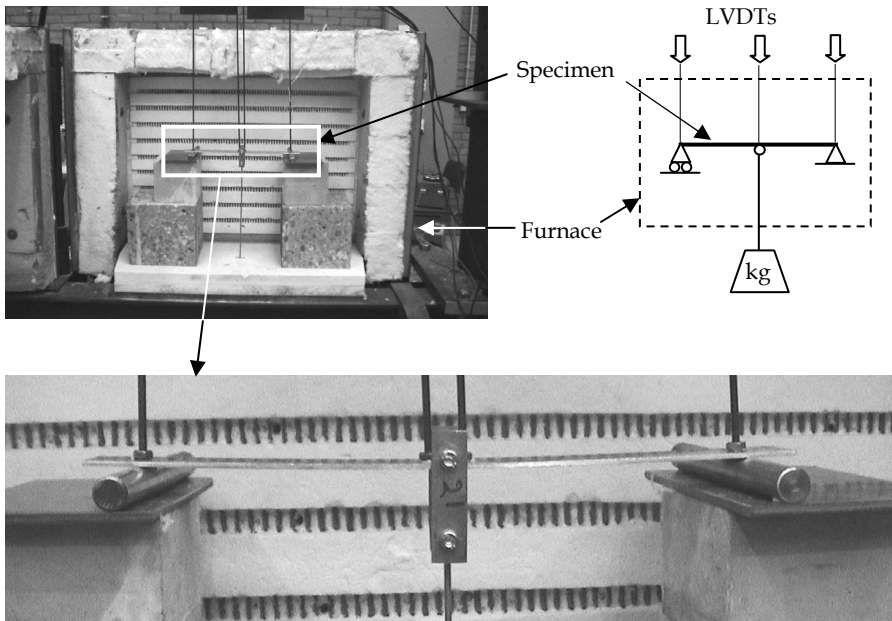


Figure 2: Overview of test set-up for bending tests

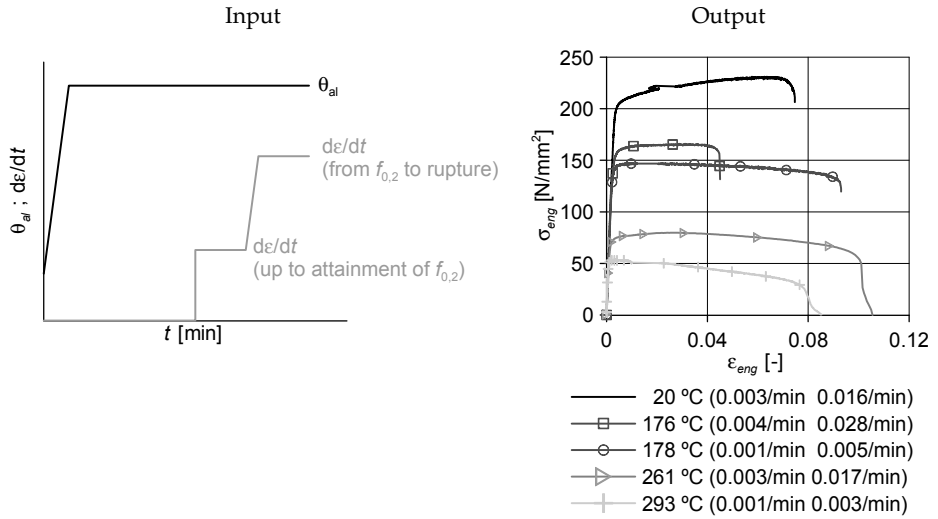


Figure 3: Examples of steady-state tensile tests on alloy 6060-T66 at elevated temperature [Maljaars, 2008]

[Kaufman, 1999] documented steady state tensile test results of 158 different alloys and tempers at various elevated temperatures. The black curve in Figure 4 presents the average values (dots) and standard deviations (bars) of the ratio between the 0.2 % proof stress at elevated and at room temperature  $f_{0.2,\theta} / f_{0.2,20^\circ\text{C}}$  for all data listed in [Kaufman, 1999]. In general the 0.2 % proof stress reduces from 80 to 20 % of the value at room temperature roughly between 175 and 350 °C. For comparison, the figure also gives the ratio  $E_\theta / E_{20^\circ\text{C}}$ .

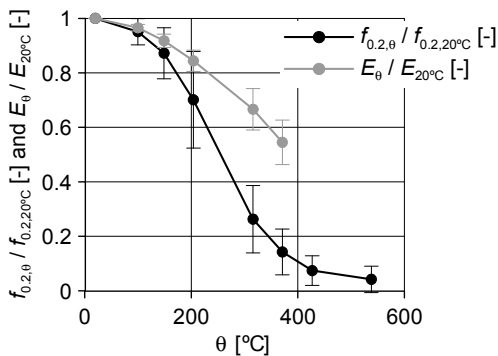


Figure 4: Ratios  $f_{0.2,\theta} / f_{0.2,20^\circ\text{C}}$  and  $E_\theta / E_{20^\circ\text{C}}$  with thermal exposure period = 30 minutes and  $d\varepsilon/dt = 0.005/\text{min}$  (data source [Kaufman, 1999])

Figure 4 shows that the scatter in ratios  $f_{0.2,\theta} / f_{0.2,20^\circ\text{C}}$  is large. However, the scatter is remarkably small when only considering alloys in the same series and the same temper - i.e. with comparable chemical composition and treatment. As an example Figure 5 presents data for the widely applied alloys 6xxx-T6 listed in [Kaufman, 1999]. Although  $f_{0.2,20^\circ\text{C}}$  varies between alloys (Figure 5a),  $f_{0.2,\theta} / f_{0.2,20^\circ\text{C}}$  is almost independent of the alloy (Figure 5b). For 5xxx alloys in temper O the scatter is slightly larger - although small compared to the scatter in  $f_{0.2,20^\circ\text{C}}$  (Figure 6). This indicates that data obtained by tests on one alloy are representative for other alloys in the same series and with the same temper. This can be used for alloys not yet tested at elevated temperature.

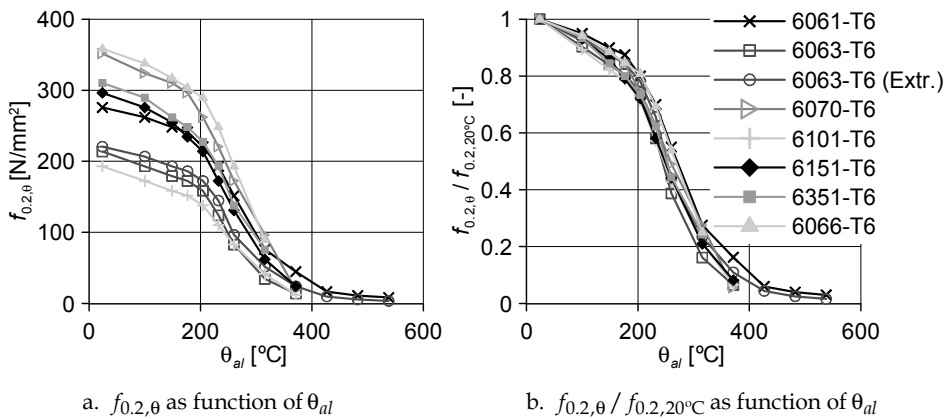


Figure 5: 0.2 % proof stress as a function of temperature of alloys in series 6xxx with temper T6

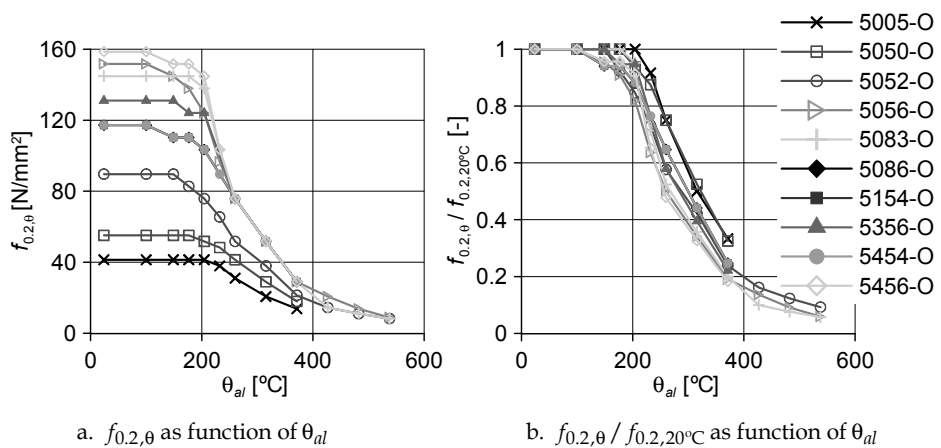


Figure 6: 0.2 % proof stress as a function of temperature of alloys in series 5xxx with temper O

### 3.4 Constitutive model in a FSE approach

Three types of tests exist for the determination of the constitutive properties:

- Steady state tests – controlled by a constant temperature and strain rate. Test output is the stress. This type of tests is discussed in Section 3.3;
- Transient state tests – controlled by an increasing temperature and a constant force or stress. Test output is the strain. Figure 7 presents an example;
- Creep tests – controlled by a constant temperature and a constant force or stress. Test output is the strain.

Transient state and creep tests are discussed in this section.

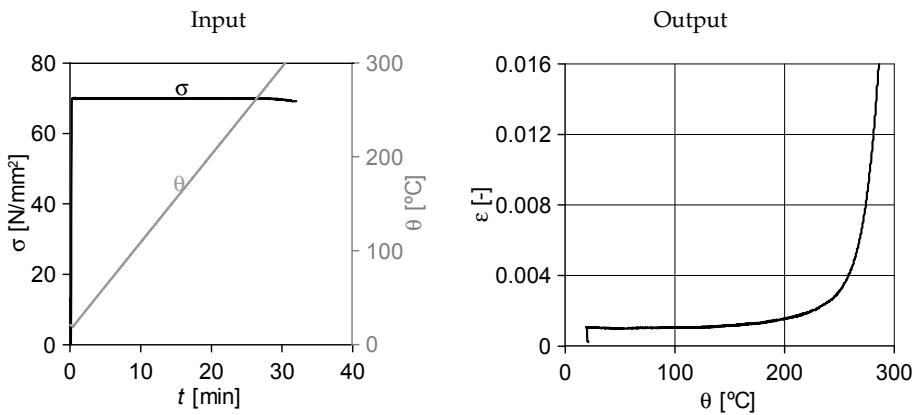


Figure 7: Example of a uniaxial transient state test on alloy 5083-O/H111 [Maljaars et al., 2008]

The resulting stress-strain relationships of steady state tests may differ from those of transient state tests due to the influence of creep. Transient state test conditions are generally regarded as better approaching fire conditions than steady-state test conditions. Steady state tests may provide constitutive properties that are accurate enough for the “traditional” fire design approach. The FSE approach may require more realistic data. For this reason stress-strain relationships are derived based on transient state conditions in [Maljaars et al., 2008]. The procedure comprises the following steps:

1. Creep tests were carried out with a stepwise increasing temperature and a constant force or vice versa. An example is given in Figure 8;
2. The strain rates determined in step 1 were used to calibrate an existing constitutive model by Dorn and Harmathy [Dorn, 1954], [Harmathy, 1967a and 1967b);
3. The model was modified in order to better fit the test results;

4. Transient state tests were carried out to validate the modified Dorn-Harmathy model.

The modified Dorn-Harmathy model is based on the approximation that the mechanical strain  $\varepsilon_{\theta}$  at elevated temperature consists only of elastic strain  $\varepsilon_{el,\theta}$  and permanent creep strain  $\varepsilon_{t,\theta}$  (Equation (6)). Equation (7) describes the creep strain  $\varepsilon_{t,\theta}$ . Table 2 presents the calibrated parameters.

$$\varepsilon_{\theta} = \varepsilon_{el,\theta} + \varepsilon_{t,\theta} \quad (6)$$

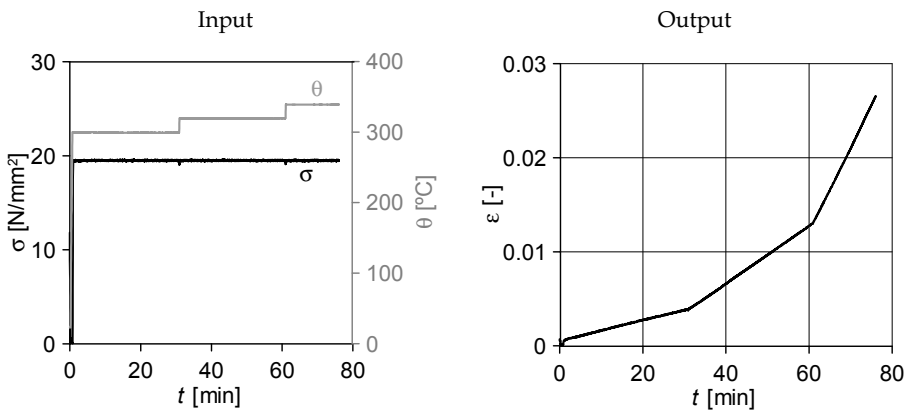


Figure 8: Temperature, stress and measured mechanical strain as a function of time in a creep test on alloy 5083-H111 with a constant temperature [Maljaars et al., 2008]

Table 2: Material dependent parameters in equations (1) to (5)

Parameter	Alloy 5083-O/H111	Alloy 6060-T66
$\varepsilon_{t,lim}$	> 0.04 [-] (i.e. irrelevant)	0.002 [-]
$C_1$ *	18282 [°C]	23453 [°C]
$C_2$	$6.7 \cdot 10^{10}$ [/min]	$7.0 \cdot 10^{12}$ [/min]
$C_3$	0.025 [-]	0.04 [-]
$C_4$	3 [-]	3 [-]
$C_5$	$4.0 \cdot 10^{-10}$ [-]	$2.0 \cdot 10^{-18}$ [-]
$C_6$	3.4 [-]	7.45 [-]

\* Parameter  $C_1$  is equal to ratio between the activation energy and the universal gas constant.

$$\begin{aligned} \varepsilon_{t,\theta} \leq \varepsilon_{t,lim} : \frac{d\varepsilon_{t,\theta}}{dt} &= C_2 [\sinh(C_3 \sigma)]^{C_4} \exp\left(\frac{-C_1}{\theta_{al} + 273^\circ\text{C}}\right) \coth^2\left(\frac{\varepsilon_{t,\theta} + 1 \cdot 10^{-7}}{C_5 \sigma^{C_6} + 1 \cdot 10^{-7}}\right) \\ \varepsilon_{t,\theta} > \varepsilon_{t,lim} : \frac{d\varepsilon_{t,\theta}}{dt} &= C_2 [\sinh(C_3 \sigma)]^{C_4} \exp\left(\frac{-C_1}{\theta_{al} + 273^\circ\text{C}}\right) \coth^2\left(\frac{\varepsilon_{t,\theta} + 1 \cdot 10^{-7}}{C_5 \sigma^{C_6} + 1 \cdot 10^{-7}}\right) \frac{\varepsilon_{t,\theta}}{\varepsilon_{t,lim}} \end{aligned} \quad (7)$$

Equation (7) is an implicit equation where the creep strain rate depends on the creep strain already developed. A numerical procedure is used to determine the creep strain at the end of each timestep  $i$  based on the creep strain of the previous timestep  $i-1$  and the creep strain increment (Equation (8)). These equations may be applied in FE programmes for the evaluation of structural behaviour in a FSE approach.

$$\begin{aligned} \varepsilon_{t,\theta}^{i-1} \leq \varepsilon_{t,lim} : \varepsilon_{t,\theta}^i &= \varepsilon_{t,\theta}^{i-1} + C_2 [\sinh(C_3 \sigma)]^{C_4} \exp\left(\frac{-C_1}{\theta_{al} + 273^\circ\text{C}}\right) \coth^2\left(\frac{\varepsilon_{t,\theta}^{i-1} + 1 \cdot 10^{-7}}{C_5 \sigma^{C_6} + 1 \cdot 10^{-7}}\right) \Delta t \\ \varepsilon_{t,\theta}^{i-1} > \varepsilon_{t,lim} : \varepsilon_{t,\theta}^i &= \varepsilon_{t,\theta}^{i-1} + C_2 [\sinh(C_3 \sigma)]^{C_4} \exp\left(\frac{-C_1}{\theta_{al} + 273^\circ\text{C}}\right) \coth^2\left(\frac{\varepsilon_{t,\theta}^{i-1} + 1 \cdot 10^{-7}}{C_5 \sigma^{C_6} + 1 \cdot 10^{-7}}\right) \Delta t \frac{\varepsilon_{t,\theta}^{i-1}}{\varepsilon_{t,lim}} \end{aligned} \quad (8)$$

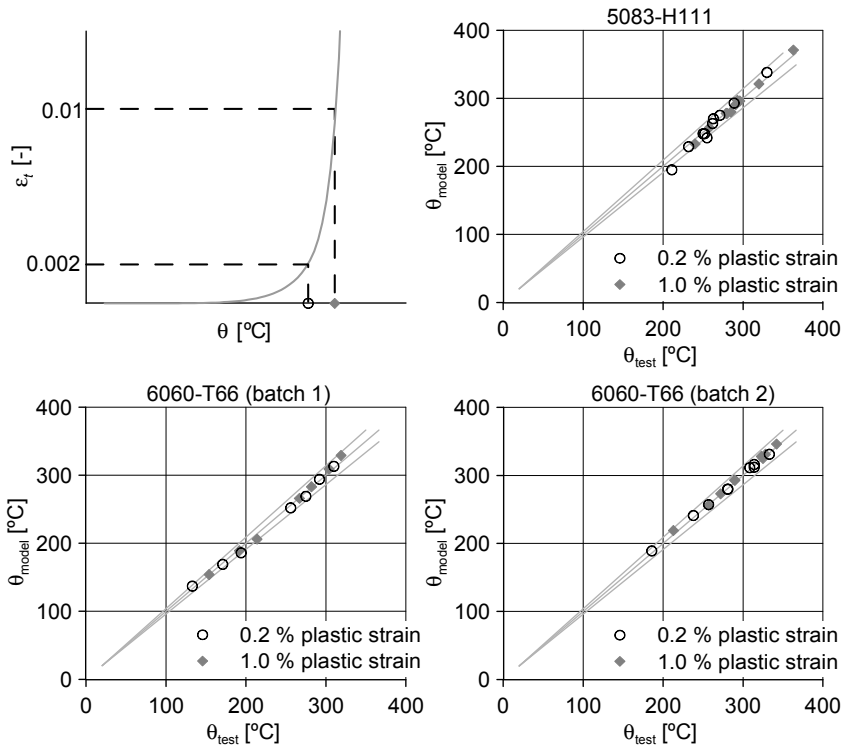


Figure 9: Agreement between transient state tests and simulations at plastic strains of 0.2 % and 1.0 %

Twenty-seven uniaxial transient state tensile tests were carried out for the validation of the model (step 4). These tests were simulated using equation (8) in a simple spreadsheet. Figure 9 gives the agreement between the tests and the simulations of the temperature at which a plastic strain of 0.2 or 1.0 % is detected. The lines in the graph indicate a deviation between the test temperature  $\theta_{test}$  and the temperature of the simulations  $\theta_{model}$  of -5 %, 0 % and +5 % (determined from 20 °C onwards). In all cases, a good agreement is observed between the measured and the simulated temperatures. Hence the model accurately represents the constitutive behaviour of aluminium alloys in fire conditions.

### 3.5 Transient state stress-strain relationships

Based on the constitutive model, it is possible to derive stress-strain curves that can be used in a “traditional” fire design approach. Such transient-state stress-strain curves are more accurate for fire conditions than the steady-state stress strain curves of Section 3.3 because creep strain evolving during the fire is accounted for in the transient-state stress-strain curves. Simulations are carried out with a certain heating rate (Figure 10a) and

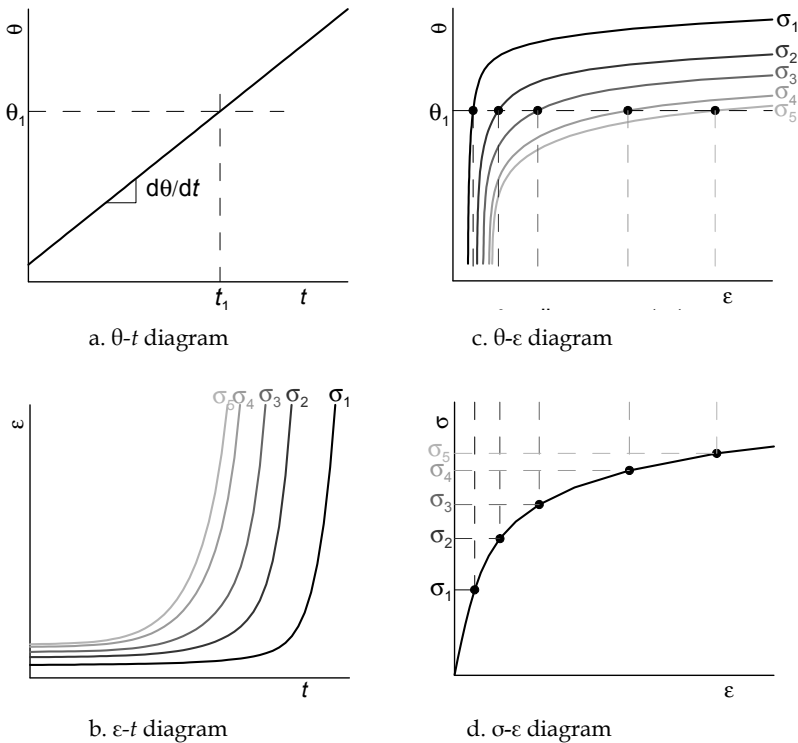


Figure 10: Derivation of a stress-strain relationship based on transient state conditions

various stress levels. Each simulation gives a strain-time curve (Figure 10b). These can also be plotted as a function of temperature (Figure 10c). Combining the stress-strain points at the same temperature and heating rate leads to a stress-strain relationship (Figure 10d). This stress-strain relationship is valid for the heating rate and exposure period considered. A similar procedure is followed for deriving the stress-strain relationships of carbon steel in [Witteveen and Twilt, 1975].

The resulting transient state stress-strain curves not only depend on the temperature, but also on the stress and temperature history. To illustrate this Figure 11a gives 4 different heating curves. In cases 1, 2 and 3, the end temperature of 275 °C is reached after 30 min while in case 4, 275 °C is reached after 120 min. Figure 11b gives the stress-strain curves at 275 °C for a constant stress in time and for the heating rates of Figure 11a. The significant difference in stress-strain curves is due to the different evolvement of creep strain in time.

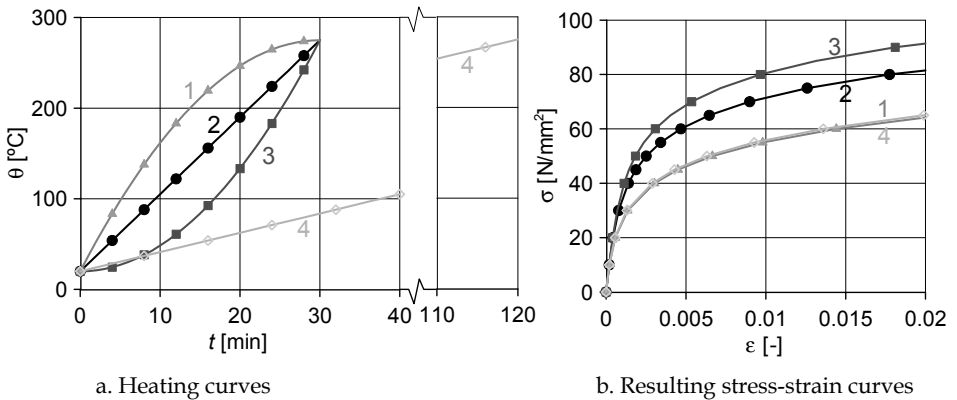


Figure 11: Examples of transient state stress-strain curves of 5083-O/H111 at a temperature of 275 °C

Heating rates are determined for a large number of natural fires in a parameter study [Maljaars et al., 2006]. Stress-strain curves are determined for these heating rates and for constant stress in time by using the above procedure. Subsequently, for each temperature the average value for  $f_{0.2,\theta}$  is determined. For most natural fires investigated, the resulting value for  $f_{0.2,\theta}$  was reasonably close to the average value – with a bandwidth of approximately  $\pm 15\%$ . The average values for the ratio  $f_{0.2,\theta} / f_{0.2,20^\circ\text{C}}$  are presented in Figure 12. Note that the curves in Figure 12 are valid only for a constant stress in time.

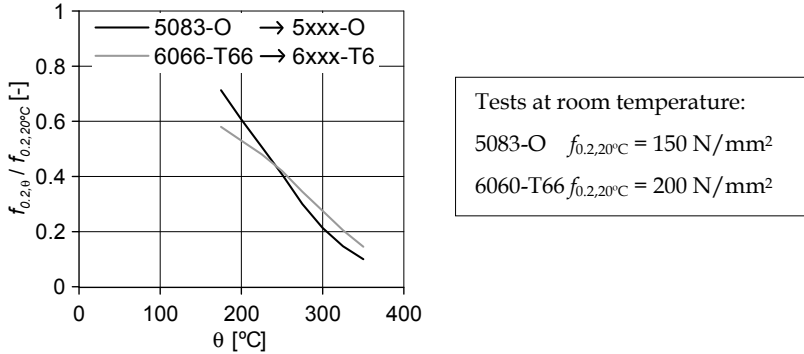


Figure 12: Reduction of the 0.2 % proof stress for transient state conditions with constant stress in time

Figures 5 and 6 showed that the ratio  $f_{0.2,\theta} / f_{0.2,20^\circ\text{C}}$  is similar for alloys in the same series and with the same temper in case of steady state conditions. Data in [Kaufman, 1999] indicate that also the amount of creep strain development is similar for alloys in the same series and with the same temper. Thus, in absence of transient state tensile tests on other alloys, the reduction in 0.2 % proof stress in Figure 12 provides an approximation for the reduction for other alloys in the same series and with the same temper.

Figure 11 shows that the transient state stress-strain curves are significantly curved. Curved stress-strain curves can be described by the Ramberg-Osgood relationship (Equation (9)). Parameter  $n_\theta$  is determined by curve fitting and describes the roundness of the curve, i.e. a more curved relationship results in a lower value for  $n_\theta$ .

$$\varepsilon = \frac{\sigma}{E_\theta} + 0.002 \left( \frac{\sigma}{f_{0.2,\theta}} \right)^{n_\theta} \quad (9)$$

Despite the differences in curves for different heating rates (Figure 11b), the values for  $n_\theta$  appear being almost independent of the heating rate for the same end temperature. Equations (10) and (11) are selected such as to give good agreement between the Ramberg Osgood stress-strain curves and the original stress-strain curves for strains up to 1 %. The stress-strain curves of fire exposed aluminium alloys can be described with equations (4), (5), (9), (10) and (11) and Figure 12.

$$\text{Alloy 5083-O/H111: } n_{\theta} = 8.8 - 0.016 \theta \quad \text{for } 175 \text{ }^{\circ}\text{C} \leq \theta \leq 350 \text{ }^{\circ}\text{C} \quad (10)$$

$$\text{Alloy 6060-T66: } n_{\theta} = 19 - 0.04 \theta \quad \text{for } 175 \text{ }^{\circ}\text{C} \leq \theta \leq 350 \text{ }^{\circ}\text{C} \quad (11)$$

## 4 Structural behaviour

### 4.1 Simple calculation models in a “traditional” fire design strategy

In a “traditional” fire design strategy the structure is usually considered as being composed of individual components such as beams, columns and connections. For each individual component the resistance at elevated temperature is checked against its load effect. [EN 1999-1-2, 2007] allows for a number of simplifications using this component approach:

- Only the effects of thermal deformations resulting from thermal gradients across the cross-section need to be considered. The effects of axial or in-plane thermal expansions may be neglected;
- The boundary conditions at supports and ends of members may be assumed to remain unchanged throughout the fire exposure.

These simplifications imply a relatively easy determination of the distribution of forces and moments. This distribution is determined with the loads in fire conditions and with a static scheme of the structure that is equal to the static scheme at room temperature.

[EN 1999-1-2, 2007] provides simple calculation models for tension members, beams, columns, beam-columns and connections. The simple calculation models deal as follows with thermal gradients across the cross-section in case these are present:

- Members not subjected to buckling phenomena (i.e. in case of tension members and class 1 and class 2 beams restrained for lateral-torsional buckling): the contribution to the cross-sectional resistance of each part of the cross-section with a certain temperature is determined by multiplying the 0.2 % proof stress at that temperature with the area of this part.
- Members subjected to buckling (i.e. columns, class 3 and class 4 beams and beams subjected to lateral-torsional buckling): the maximum temperature of the cross-section is considered. The resistance is determined for the case with a uniform temperature across the cross-section equal to this maximum temperature.

Three important failure mechanisms are considered below in detail. These mechanisms are flexural buckling, local buckling and heat affected zone rupture.

### Flexural buckling of columns

Equation (12) is provided in [EN 1999-1-2, 2007] for the buckling resistance of columns.

$$F_{u,\theta} = \chi_{20^\circ\text{C}} A f_{0.2,\theta} \frac{1}{1.2 \gamma_{fi}} \quad (12)$$

The partial safety factor  $\gamma_{fi}$  is set to unity. The equation is based on two gross approximations:

1. Factor 1.2 in equation (12) is a reduction factor taking account of the temperature dependent creep of aluminium. However, the factor is not accounting for different creep evolution at different temperatures, for different heating and/or loading rates and for different alloys.
2. The relative buckling resistance is taken equal to the value at room temperature:  $\chi_\theta = \chi_{20^\circ\text{C}}$ . This is based on the assumption that the reduction as a function of temperature of the modulus of elasticity  $E_\theta / E_{20^\circ\text{C}}$  is equal to the reduction of the 0.2 % proof stress  $f_{0.2,\theta} / f_{0.2,20^\circ\text{C}}$ . A consequence of this assumption is that the relative slenderness at elevated temperature equals the relative slenderness at room temperature:  $\lambda_{rel,\theta} = \lambda_{rel,20^\circ\text{C}}$ . Further, the relationship between  $\lambda_{rel,\theta}$  and  $\chi$  - i.e. the buckling curve - is taken equal as at room temperature. However, Figure 4 shows that  $E_\theta / E_{20^\circ\text{C}}$  reduces less fast as compared to  $f_{0.2,\theta} / f_{0.2,20^\circ\text{C}}$ . Consequently, the assumption that  $\lambda_{rel,\theta} = \lambda_{rel,20^\circ\text{C}}$  is a conservative approximation. A note in the standard addresses this issue by stating that the National Annex may give provisions to take the actual drop in modulus of elasticity into account in the design model.

A more refined calculation model is developed allowing for the above points [Maljaars et al., 2009c]. The influence of creep is implicitly taken into account in the derivation of the transient-state stress-strain curves (Section 3.5). The new calculation model is based on these stress-strain curves, meaning that an explicit creep factor in the model is not required. The model consists of three steps:

1. An analytical model for the critical buckling load of columns with a curved stress-strain relationship is proposed by [Shanley, 1947]. This so-called inelastic critical buckling load  $F_{cr,inel,\theta}$  is represented by Equation (13). The equation uses the tangential stiffness  $E_{T,\theta}$ , defined according to Equation (14).

$$F_{cr,inel,\theta} = \frac{\pi^2 E_{T,\theta} I}{L_{buc}^2} \quad (13)$$

$$E_{T,\theta} = \frac{d\sigma}{d\varepsilon} \quad (14)$$

The tangential stiffness is expressed by the parameters of the Ramberg-Osgood relationship of equation (9):

$$E_{T,\theta} = \frac{E_\theta}{1 + \frac{E_\theta 0.002 n_\theta}{f_{0.2,\theta}} \left(\frac{\sigma}{f_{0.2,\theta}}\right)^{n_\theta - 1}} \quad (15)$$

Applying Equation (15) into Equation (13) and substitution of  $\sigma$  by  $F_{cr,inel,\theta} / A$  results in:

$$\frac{F_{cr,inel,\theta}}{A} + 0.002 E_\theta n_\theta \left(\frac{F_{cr,inel,\theta}}{f_{0.2,\theta} A}\right)^{n_\theta} = \frac{\pi^2 E_\theta I}{A L_{buc}^2} \quad (16)$$

Knowing the parameters of the Ramberg-Osgood relationship  $E_\theta$ ,  $f_{0.2,\theta}$  and  $n_\theta$  and the geometrical properties  $I$  and  $A$ , Equation (9) is used to determine  $F_{cr,inel,\theta}$ . An iterative procedure is required for solving this implicit equation.

2. The inelastic relative slenderness  $\lambda_{rel,inel,\theta}$  is determined according to Equation

$$\lambda_{rel,inel,\theta} = \sqrt{\frac{A f_{0.2,\theta}}{F_{cr,inel,\theta}}} \quad (17)$$

3. A buckling curve is defined giving the relationship between the inelastic relative slenderness  $\lambda_{rel,inel,\theta}$  and the relative buckling resistance  $\chi_\theta$ . Equation (18) describes the relationship and it is presented by the curve in Figure 13.

$$\chi_\theta = \frac{1}{\lambda_{rel,inel,\theta}^2} - \frac{0.8}{\lambda_{rel,inel,\theta}^3} + \frac{0.8}{\lambda_{rel,inel,\theta}^4} \quad (18)$$

The buckling curve is based on a curve fit of the results of a parametric study with a finite element model. Experiments by [Langhelle, 1999] and [Langhelle et al., 1996] on aluminium columns at elevated temperatures are used for the validation of the finite element model. The validation and the cases considered in the parameter study are presented in [Maljaars et al., 2009c]. The results of the parametric study are indicated with symbols in Figure 13. The ultimate buckling resistance according to the new design model for flexural buckling of fire exposed aluminium columns is given by equation (19).

$$F_{u,\theta} = \chi_\theta A f_{0,2,\theta} \frac{1}{\gamma_{fi}} \quad (19)$$

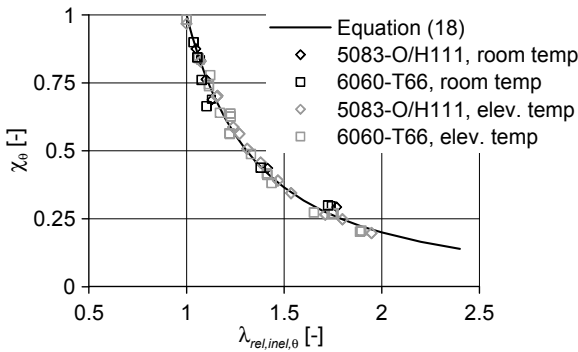


Figure 13: Relationship between relative buckling resistance and inelastic relative slenderness

#### Local buckling of plates and sections in compression

[EN 1999-1-2, 2007] does not provide a simple calculation model for local buckling of class 4 plates and sections of aluminium exposed to fire conditions. Such a model was also not found in other standards. A simple calculation model was developed by [Maljaars et al.,

2010], following a similar procedure as for flexural buckling of columns described above. The model consists of three steps:

1. An analytical model for the critical buckling stress of plates with a curved stress-strain relationship is proposed by [Stowell, 1948]. This inelastic critical buckling load  $\sigma_{cr,inel,\theta}$  is represented by Equations (20) and (21). The equation uses the tangential stiffness  $E_{T,\theta} = d\sigma / d\varepsilon$  and the secant stiffness  $E_{S,\theta} = \sigma / \varepsilon$ .

$$\sigma_{cr,inel,\theta} = k_{cr} \frac{\pi^2 \eta_{\theta} E_{\theta}}{12(1-\nu_{\theta}^2)} \left(\frac{t}{b}\right)^2 \quad (20)$$

$$\eta_{\theta} = \begin{cases} \frac{E_{S,\theta}}{E_{\theta}} \left( \frac{1}{2} + \frac{1}{2} \sqrt{\frac{1}{4} + \frac{3}{4} \frac{E_{T,\theta}}{E_{S,\theta}}} \right) & \text{for simply supported internal plates} \\ \frac{E_{S,\theta}}{E_{\theta}} & \text{for simply supported outstands} \end{cases} \quad (21)$$

$$k_{cr} = \begin{cases} 4 & \text{for simply supported internal plates} \\ \frac{b^2}{L^2} + 6 \frac{1-\nu_{\theta}}{\pi^2} & \text{for simply supported outstands} \end{cases} \quad (22)$$

The tangential stiffness and secant stiffness are expressed by the parameters of the Ramberg-Osgood relationship, Equations (15) and (23), respectively.

$$E_{S,\theta} = \frac{E_{\theta}}{1 + \frac{E_{\theta} 0.002}{f_{0.2,\theta}} \left(\frac{\sigma}{f_{0.2,\theta}}\right)^{n_{\theta}-1}} \quad (23)$$

Equations (15) and (23) are then applied into equations (21) and (20). This leads to an extensive equation especially for internal plates. As an alternative to this extensive equation, an approximate equation is defined:

$$C E_{\theta} 0.002 \left(\frac{\sigma_{cr,inel,\theta}}{f_{0.2,\theta}}\right)^{n_{\theta}} + \sigma_{cr,inel,\theta} = k_{cr} \frac{\pi^2 E_{\theta}}{12(1-\nu_{\theta}^2)} \left(\frac{t}{b}\right)^2 \quad (24)$$

With  $C = 1.4$  for simply supported internal plates and  $C = 1.0$  for simply supported outstands. The equation gives the exact solution for simply supported outstands and is an approximation for simply supported internal plates, where

the value  $C = 1.4$  is determined by curve fitting (elaborated in [Maljaars, 2008]).

The inelastic critical stress  $\sigma_{cr,inel,\theta}$  is determined with an iterative procedure using equation (24).

2. The inelastic relative slenderness  $\lambda_{cr,inel,\theta}$  is determined with Equation (25).

$$\lambda_{rel,inel,\theta} = \sqrt{\frac{f_{0,2,\theta}}{\sigma_{cr,inel,\theta}}} \quad (25)$$

3. Buckling curves are defined giving the relationship between the inelastic relative slenderness  $\lambda_{rel,inel,\theta}$  and the relative buckling resistance  $\chi_\theta$ . Equation (26) describes the relationships and they are presented by the curves in Figure 14.

$$\chi_\theta = \begin{cases} \frac{1}{\lambda_{rel,inel,\theta}} + 0.2 \frac{1}{\lambda_{rel,inel,\theta}^2} - 2.5 \frac{1}{\lambda_{rel,inel,\theta}^3} + 2.3 \frac{1}{\lambda_{rel,inel,\theta}^4} & \text{for internal plates} \\ \frac{1}{\lambda_{rel,inel,\theta}} + 1.5 \frac{1}{\lambda_{rel,inel,\theta}^2} - 0.5 \frac{1}{\lambda_{rel,inel,\theta}^3} + 3.5 \frac{1}{\lambda_{rel,inel,\theta}^4} & \text{for outstands} \end{cases} \quad (26)$$

The buckling curves are based on a curve fit of the results of a parametric study with a finite element model. Experiments by [Maljaars et al. 2009d and 2009e] on aluminium sections at elevated temperatures are used for the validation of the finite element model. The results of the parametric study are indicated with symbols in Figure 14. Equation (27) presents the ultimate buckling resistance according to the new design model for local buckling of fire exposed aluminium plates.

$$F_{u,\theta} = \chi_\theta b t f_{0,2,\theta} \frac{1}{\gamma_{fi}} \quad (27)$$

### Rupture of the heat affected zone

Alloys in series 6xxx applied in structural applications are usually hardened by a heat treatment. Alloys in series 5xxx are often hardened by cold working. When structures of hardened alloys are welded, the material close to the weld is exposed to severe heat input. This heat partially “destroys” the favourable aluminium matrix obtained by hardening so that the strength of this zone is reduced compared to the hardened parent metal. The zone with reduced strength is called the heat affected zone (HAZ). Symbol  $\rho_{0,2,HAZ} =$

$f_{0.2,haz} / f_{0.2,parent}$  is used to address the reduction of the 0.2 % proof stress. The reduction of the ultimate tensile strength is denoted with symbol  $\rho_{u,haz} = f_{u,haz} / f_{u,parent}$ .

In absence of test results, [EN 1999-1-2, 2007] does not provide values for  $\rho_{0.2,haz,\theta}$  and  $\rho_{u,haz,\theta}$  at elevated temperatures. The standard assumes that  $\rho_{0.2,haz,\theta}$  and  $\rho_{u,haz,\theta}$  at elevated temperature are equal to the values at room temperature. This is supposed to be a conservative approximation because of the following way of reasoning. When exposed to fire conditions all material is subjected to heat input. At a certain temperature, there is no difference expected between the material heated by fire and the material formerly heated

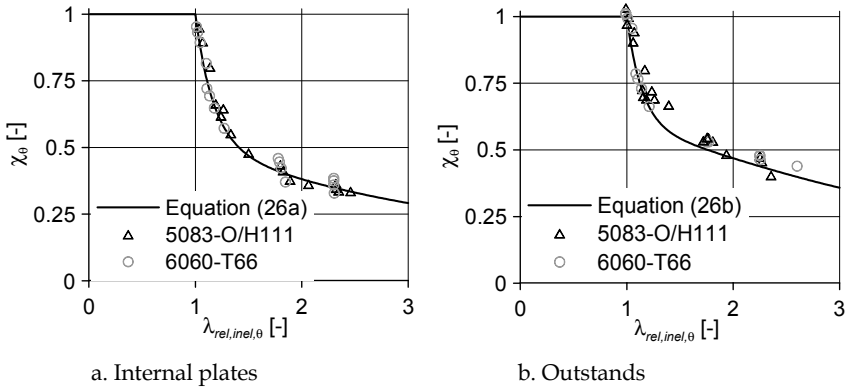


Figure 14: Relationship between relative buckling resistance and inelastic relative slenderness

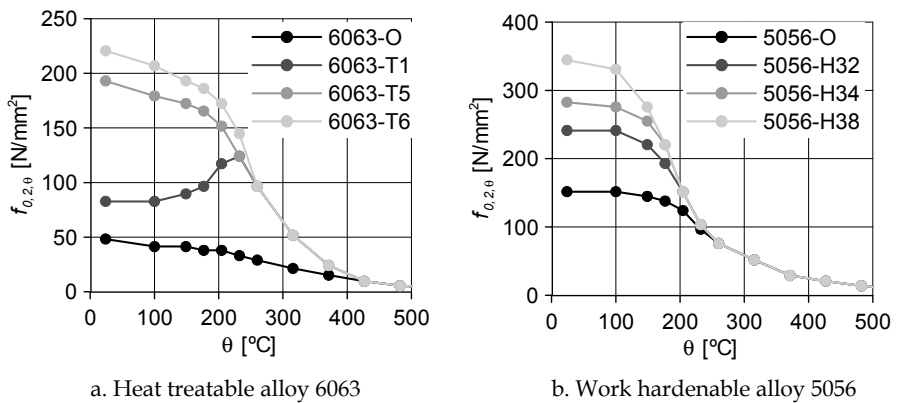


Figure 15: Steady state tensile test results at elevated temperatures for two alloys with various tempers (data source: [Kaufman, 1999])

by the welding process. Consequently,  $\rho_{0,2,haz}$  and  $\rho_{u,haz}$  tend to unity at increasing temperature. Tensile test data by [Kaufman, 1999] confirm this assumption (Figure 15). At elevated temperature, there is no longer a difference in the strength of material with different initial tempers Tx or Hxx.

A limited experimental programme was carried out on the strength of welded specimens at elevated temperatures. The programme consisted mainly of steady state tensile tests and a small number of transient-state tensile tests on unwelded specimens (results representative for parent metal) and on specimens with a fillet weld and a butt weld (results representative for HAZ). The programme and results are presented in [Maljaars and Soetens, 2009b]. Some results of the steady-state test programme are indicated in Figure 16. It shows that the strength of the HAZ equals that of the parent metal at a temperature of 300 °C i.e.  $\rho_{u,haz,300^\circ\text{C}} = 1.0$ . In the relevant temperature range of 175-300 °C, however,  $\rho_{u,haz,<300^\circ\text{C}} < 1.0$ . An approximately linear increase is found for  $\rho_{u,haz,\theta}$  between 20 °C and 300 °C. In absence of further test data, the approximation according to equation (28) is therefore recommended for 6xxx-T6 alloys.

$$\rho_{u,haz,\theta} = \begin{cases} 1 + (\rho_{u,haz,20^\circ\text{C}} - 1) \frac{300^\circ\text{C} - \theta_{al}}{300^\circ\text{C} - 20^\circ\text{C}} & \text{if } 20 \leq \theta_{al} < 300^\circ\text{C} \\ 1 & \text{if } \theta_{al} \geq 300^\circ\text{C} \end{cases} \quad (28)$$

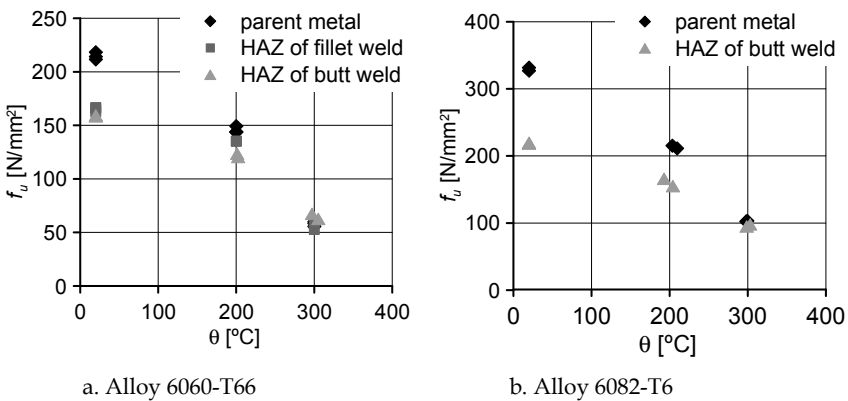


Figure 16: Steady state tensile test results at elevated temperature on parent metal and on welded specimens

#### 4.2 *Advanced calculation models in a FSE approach*

The component approach with its approximations is in most cases not recommended for application in a Fire Safety Engineering (FSE) approach. A more realistic approach is required where thermal expansion is taken into account as well as changing boundary conditions at member supports. On the one hand, restrained thermal expansion may result in internal stresses in case of statically indeterminate structures. This may cause failure in an earlier stage of the fire as compared to a theoretical case without thermal expansion. On the other hand, failure of one component does not necessarily mean failure of the entire structure. Parts that are less weakened by the fire may overtake the load of the most weakened parts, leading to redistribution of forces. Damage or collapse of individual members not leading to collapse of the entire structure is usually allowed in a fire design because the aim is preventing progressive collapse and providing safe escape routes only (free after [Franssen and Zaharia, 2006]).

Taking into account the above effects usually means that either the entire structure needs to be analysed as a whole, or the structure needs to be divided into parts with no or limited interaction with the rest of the structure and these parts need to be analysed. Simple calculation models are not available for such cases. For these cases [EN 1999-1-2, 2007] refers to “advanced” calculation models that need to be based on fundamental physical behaviour and verified on the basis of relevant test results. Some examples are given in Section 5.

## 5 **Design examples**

Two examples are elaborated in this chapter. Emphasis is on the structural response rather than on the thermal response.

### 5.1 *Column in an office building*

Consider the part of the structure of an office building according to Figure 17. The part is selected such as to have no significant structural interaction with the rest of the structure. The geometry of the beams and columns is given in Table 3. The fire scenario comprises one of the compartments being exposed to fire. In this example it is assumed that the columns and beam of the fire compartment (indicated with arrows) are completely engulfed in flames while the rest of the building remains at ambient temperature.

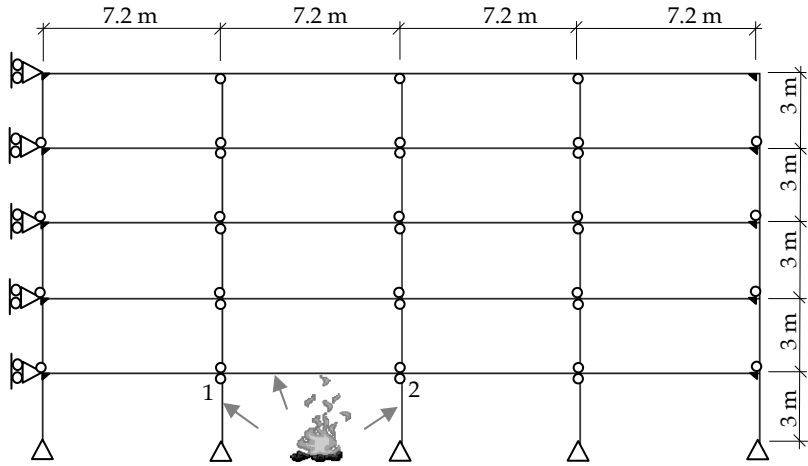
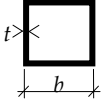
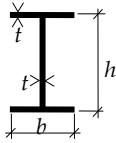


Figure 17: Compartment fire in an office building

Table 3: Cross-sectional properties of the beams and columns

Part	Shape	Dimensions	Properties
Columns		$b = 197 \text{ mm}$ $t = 4.34 \text{ mm}$	$A = 3360 \text{ mm}^2$ $I_y = 2.16 \cdot 10^7 \text{ mm}^4$
Beams		$h = 430 \text{ mm}$ $b = 260 \text{ mm}$ $t = 7 \text{ mm}$	$A = 6552 \text{ mm}^2$ $I_y = 2.05 \cdot 10^8 \text{ mm}^4$

The example considers the exposed columns. The columns are extruded profiles of alloy 6060-T66 and are insulated with glass wool with a thickness  $d_p = 24 \text{ mm}$ , properties  $\rho_p = 60 \text{ [kg/m}^3]$ ;  $c_p = 1030 \text{ [J/kg K]}$  and  $\lambda_p = 2.7 \cdot 10^{-7} \theta_{al}^2 + 1 \cdot 10^{-4} \theta_{al} + 0.031 \text{ [W/m K]}$ . The external load on the column for fire design is  $F_{S,fi} = 180 \text{ kN}$ . Load eccentricity is not considered in this example. The required fire resistance is 60 min and the partial factor is  $\gamma_{fi} = 1.0$ .

#### “Traditional” fire design approach

The member temperature is evaluated with equation (2) for the standard temperature-time curve (Figure 18a). The member temperature after 60 minutes is equal to 360 °C. The corresponding material properties are:  $E_\theta = 38000 \text{ N/mm}^2$  (Equation 5);  $f_{0.2,\theta} = 0.16 \cdot 200$

$N/\text{mm}^2 = 32 \text{ N}/\text{mm}^2$  (Figure 12) and  $n_\theta = 4.6$  (Equation 11). Note that  $\theta_{at} = 360 \text{ }^\circ\text{C}$  is just out of the application range, which is neglected here. The resistance of the column is subsequently determined:

- The resistance for flexural buckling is determined with equations (16) – (19). The results are:  $F_{cr,inel,\theta} = 98 \text{ kN}$ ;  $\lambda_{rel,inel,\theta} = 1.048$ ;  $\chi = 0.88$ ;  $F_u = 94.6 \text{ kN}$ ;
- The resistance for local buckling is determined with equations (24) – (27). The results are:  $\sigma_{cr,inel,\theta} = 26,8 \text{ N}/\text{mm}^2$ ;  $\lambda_{rel,inel,\theta} = 1.092$ ;  $\chi = 0.78$ ;  $F_u = 84.0 \text{ kN}$ .

Interaction between local and global buckling is not yet taken into account. Interaction results in a lower resistance than the resistances given here for the individual failure modes. Due to the fact that the load on the column  $F_{S,fi}$  is already larger than the resistance of the individual failure modes, the column is not able to resist the load. The conclusion is that the column fails before reaching the required fire resistance of 60 min.

#### FSE approach

The natural fire gas temperature is determined for a compartment lay-out and a fire load typical for an office building in [Maljaars et al., 2006], using the programme Ozone V2.1 [Cadorin et al., 2004]. Equation (2) is used to determine the member temperature, however the thermal capacity of the fire insulation material is neglected, i.e.  $\phi = 0$ . The gas and member temperatures are given in Figure 18b. The maximum member temperature during 60 minutes of fire exposure is equal to  $200 \text{ }^\circ\text{C}$ .

The column is partially restrained for thermal expansion in axial direction. This has to be taken into account in the evaluation of the resistance. As simple design models that take this into account do not exist, the resistance is evaluated on the basis of FE models. A model of the entire structure, with the members modelled in such detail that also failure mechanisms such as local buckling are considered, is too time-consuming for practice. For this reason, the following approach is applied:

- The structure of Figure 17 is modelled in the FE programme DIANA v. 9.2 [De Witte and Kikstra, 2007] with simple beam elements. The material properties consist of linear elasticity at room temperature combined with the coefficient of linear thermal expansion. In the analysis, the exposed beams and columns obtained a temperature increase. The result of the analysis is the vertical displacement of the nodes 1 and 2 in Figure 17 and the reaction forces in the heated members. The spring stiffness exerted by the rest of the building on the

heated columns is determined by dividing the reaction forces by the displacements. This spring stiffness is equal to  $k = 826 \text{ N/mm}$ ;

- The heated column is modelled in detail with 8-noded shell elements in DIANA v. 9.2. A spring is applied at the column end in axial direction with  $k = 826 \text{ N/mm}$ . The external load  $F_{S,fi} = 180 \text{ kN}$  is applied at the same position. An initial geometrical imperfection pattern is applied consisting of the summation of the following two imperfection patterns:

- The first Euler buckling mode of the column for local buckling, scaled in such a way that the maximum imperfection is equal to  $b / 500$ .
- The first Euler buckling mode of the column for flexural buckling, scaled in such a way that the maximum imperfection is equal to  $L / 500$ .

The material model given by equation (8) is applied directly into the finite element program via a user supplied subroutine. Thermal expansion is also applied. Finally the external load is applied onto the column and the column is heated with the curve in Figure 18b.

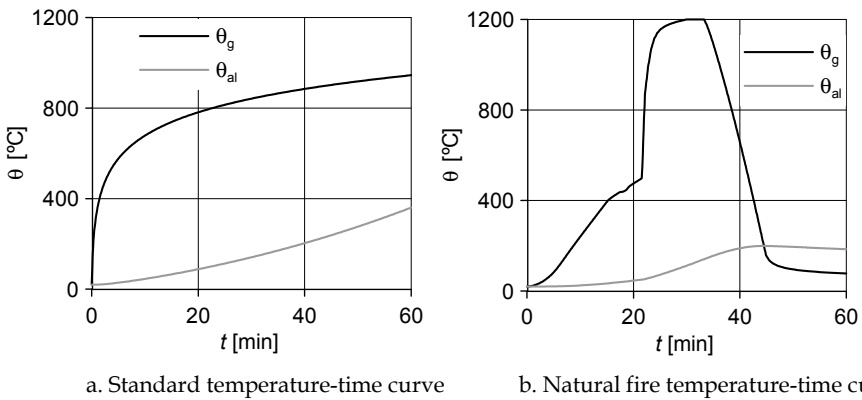


Figure 18: Temperature development in design example 1

The finite element model at  $t = 45 \text{ min}$  is presented in Figure 19a (with deformations exaggerated). Figure 19b shows the axial deformation of the member  $u$  as a function of time. Load application at  $t = 0$  results in a negative deformation. Thermal expansion causes a positive deformation during heating. Creep deformations appear being smaller than thermal deformations for this member. The conclusion is that the member survives this fire thus the fire resistance is sufficient.

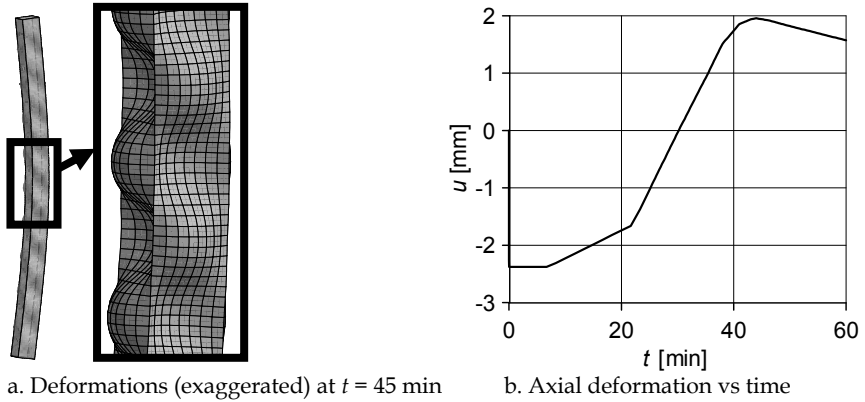


Figure 19: Results of the FE model of the exposed column in design example 1

### 5.2 Atrium roof in a shopping mall

Consider the shopping mall according to Figure 20. The roof of the atrium consists of aluminium frames with fire resistant glass panels. The aluminium bars (Figure 20c) have a distance in between of 0.82 m and are hinged supported about the strong and weak axes at both ends. The fire scenario comprises a fire in Shop 1.

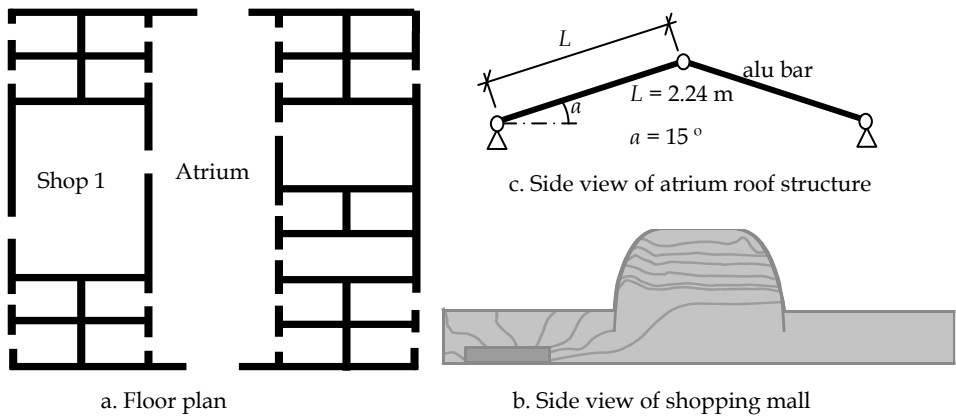


Figure 20: Lay-out of the shopping mall

The example considers the non-insulated bars of the atrium roof. These are extruded rectangular hollow sections of alloy 6060-T66 with dimensions 75 mm x 37.5 mm x 4 mm. The external load in fire condition is a distributed load of 0.43 kN/m acting in vertical direction. The required fire resistance is 30 min and the partial factor is  $\gamma_{fi} = 1.0$ .

### “Traditional” fire design approach

Equation (1) is applied for determining the member temperature for exposure to the standard temperature-time curve. The bar is evaluated as exposed at 3 sides because the upper part of the bar is located outside. The resulting aluminium temperature reaches the melt temperature (appr. 600 °C) after 11 minutes of exposure to the standard fire. Hence the fire resistance of the atrium roof structure is insufficient.

### FSE approach

The natural fire gas temperature is determined with a zone model in [Twilt and Van Oerle, 1999]. Figure 21a presents the resulting gas temperature just below the roof structure. The gas temperature is (almost) steady state with a maximum of 280 °C. The lower part of the bar is directly exposed to this temperature while the upper part is outside. Thermal bending of the member is expected due to the unequal temperature distribution over the cross-section. The glass panel might not be able to follow the thermal deformation of the bar. This may result in openings between the member and the glass panel, which in turn influences the temperature of the member. It is possible to accurately determine the temperature of the bar with a coupled thermal – mechanical model. This is not applied in this example. Instead, two extreme cases are considered for the member temperature:

- In case 1 a temperature of 280 °C is assumed for the bottom part and 20 °C is assumed for the upper part of the bar, with an abrupt temperature change at the junction between the exposed part and the outside part, Figure 21b case 1.
- In case 2 a temperature of 280 °C is assumed for the entire bar, Figure 21b case 2.

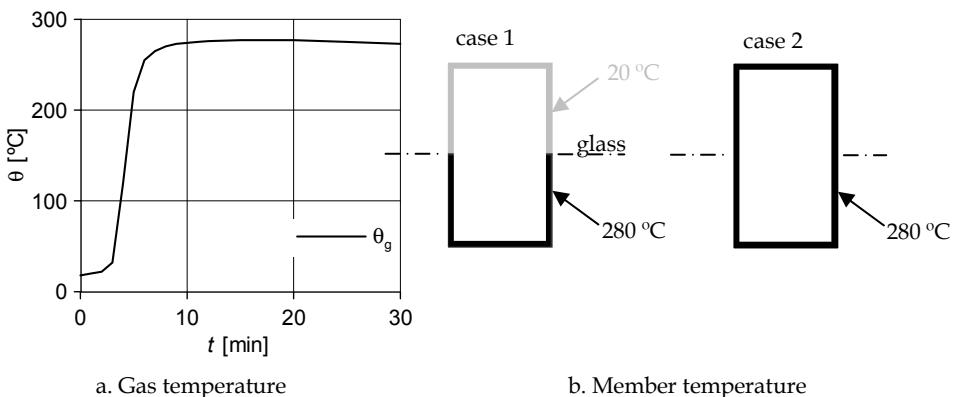


Figure 21: Temperature development in the FSE approach for design example 2

The bar is hinged in both directions so there is no interaction with the rest of the structure. The bar is subjected to a combination of bending moment and normal force. [EN 1999-1-2, 2007] provides a simple calculation model for such a beam column. However, this calculation model assumes a uniform temperature through the section equal to the maximum temperature of the member. On the one hand this may be a conservative assumption for the case 1 member temperature because  $f_{0,2,\theta}$  at maximum temperature is lower than  $f_{0,2,\theta}$  at average temperature. On the other hand the thermal bending of the bar causes an increase of the second order bending moment due to the normal force acting on the bar (Figure 22a). The temperature distribution also results in internal stresses. These effects have a reducing effect on the member resistance. Hence the simple calculation model only gives an approximation of the real structural behaviour in fire for the case 1 member temperature.

In order to accurately determine the fire resistance, a FE model is developed for the bar. The material model given by equation (8) is applied as well as thermal expansion. Finally the external load is applied. Bending of the bar with case 1 member temperature caused by thermal expansion is presented in Figure 22b (deflection not scaled). The FE results indicate that the deflection due to thermal bending is 20 times larger than the deflection due to the external load at room temperature. The ratio between the thermal deflection and the span is 1/40. This may result in breaking of the glass panels if the connection between the bar and the panel is too stiff and strong. In this example the effect of thermal bending on the glass panels is not examined further; the analysis concentrates on the fire resistance of the bar itself.

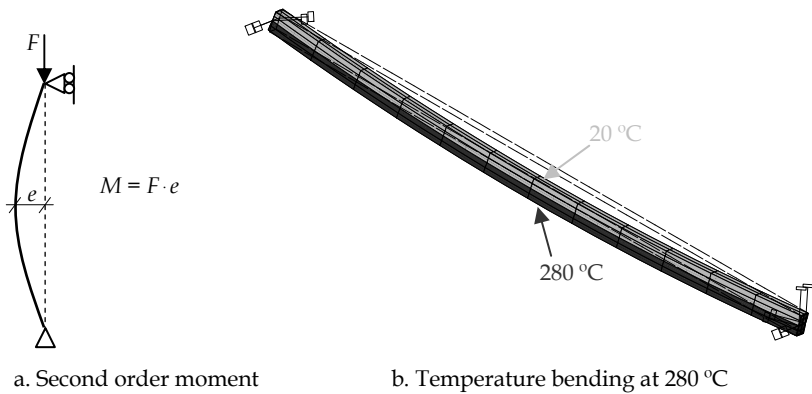


Figure 22: Temperature bending effect on member resistance for case 1 member temperature

The FE analyses showed that the mechanical deflection after 30 minutes of fire exposure is relatively small (approximately 1 mm) for both temperature cases. The real temperature distribution is expected being in between these extreme cases. Thus the conclusion is that the bar resists the load during the required fire resistance period of 30 minutes. The fire resistance of the bar is sufficient.

### 5.3 *Remark on the reliability*

Most modern structural codes and rules for design at room temperature are related implicitly or explicitly to satisfying a certain reliability level. In case of a traditional fire design, the reliability is actually unknown. Experience with this approach has learnt that it results in an acceptable safety level. Such experience is not available in case of a FSE approach. In a proper FSE approach the reliability should be determined and checked to a target value. Such a reliability study has not been carried out in the current study and it is a recommendation for future research. First steps in this future research should be to determine the distributions of probability for relevant parameters and to determine the reliability of the models involved.

## 6 **Conclusions**

- The strength of aluminium reduces at moderately elevated temperatures (roughly between 175 °C and 350 °C). This is the main reason that aluminium structures are relatively sensitive to fire exposure;
- Fire Safety Engineering (FSE) provides a more accurate approximation of the real behaviour in fire as compared to a traditional fire design. Due to the sensitivity of aluminium for fire conditions, a realistic – not too conservative – approximation of the real behaviour is often required in order to be a realistic alternative as structural material. For this reason, FSE is an excellent method to evaluate the fire resistance of aluminium structures;
- Fire insulation materials suited for aluminium structures should be effective in the range of 175 – 350 °C should have a low density, a low thermal conductivity and should be flexible enough to follow the relatively large thermal- and creep deformations of aluminium;
- The modified creep model by Dorn and Harmathy provides a sound basis for deriving transient state stress-strain relationships of fire exposed aluminium alloys;

- The relative value of the 0.2 % proof stress - i.e. the ratio  $f_{0.2,20^{\circ}\text{C}} / f_{0.2,\theta}$  - determined in tests for a limited number of alloys are representative for all alloys in the same series and with the same temper;
- Transient state stress-strain relationships at elevated temperatures are significantly curved; much more than at room temperature. Simple calculation models for flexural buckling and local buckling have been developed in which the curvature of the stress-strain relationship is explicitly taken into account;
- The difference in strength between the HAZ and parent metal gradually disappears at increasing temperature. Preliminary tests show that the HAZ strength is equal to the strength of the parent metal at temperatures of 300 °C and higher;
- Numerical models using the modified Dorn-Harmathy constitutive model provide a powerful tool to determine the fire resistance with respect to the load-bearing function of aluminium structures, based on FSE;

### *Acknowledgement*

Part of this research was carried out under the project number MC1.02147 in the framework of the Research Program of the Materials Innovation Institute M2i ([www.m2i.nl](http://www.m2i.nl)), the former Netherlands Institute for Metals Research.

The members of the joint-industry project group “Fire Design of Aluminium Structures”, The Netherlands, are kindly acknowledged for their contribution.

## Symbol list

### Main symbols

$\alpha$	=	Coefficient of linear thermal expansion [-]
$\alpha_c$	=	Convection coefficient [ $W/m^2 K$ ]
$\gamma$	=	Partial factor [-]
$\rho$	=	Density [ $kg/m^3$ ]
$\rho_{0.2,haz}$	=	Reduction factor for the 0.2 % proof stress due to the HAZ [-]
$\rho_{u,haz}$	=	Reduction factor for the tensile strength due to the HAZ [-]
$\varepsilon$	=	Emissivity [-] or Strain [-]
$\varepsilon_{el}$	=	Instant elastic strain [-]
$\varepsilon_t$	=	Creep strain [-]
$\varepsilon_{t,lim}$	=	Creep strain at the start of the tertiary creep stage [-]
$\varepsilon_{th}$	=	Thermal strain (strain due to thermal expansion) [-]
$\nu$	=	Poisson ratio [-]
$\chi$	=	Relative buckling resistance (buckling resistance divided by plastic capacity) [-]
$\sigma$	=	Stress [ $N/mm^2$ ]
$\theta$	=	Temperature [ $^{\circ}C$ ]
$\lambda$	=	Thermal conductivity [ $W/m K$ ]
$\lambda_{rel}$	=	Relative slenderness [-]
$\Delta t$	=	Time interval [s], taken max. 5 s in eq. (1) and 30 s in eq. (2).
$A$	=	Section area [ $mm^2$ ]
$A_m/V$	=	Section factor for unprotected members (exposed surface over volume);
$A_p/V$	=	Section factor for protected members;
$b$	=	Plate width [mm]
$c$	=	Specific heat [ $J/kg K$ ]
$E$	=	Modulus of elasticity [ $N/mm^2$ ]
$E_S$	=	Secant modulus of elasticity [ $N/mm^2$ ]
$E_T$	=	Tangential modulus of elasticity [ $N/mm^2$ ]
$f_{0.2}$	=	0.2 % proof stress [ $N/mm^2$ ]

$f_2$	=	2 % proof stress [N/mm <sup>2</sup> ]
$F_u$	=	Flexural or local buckling resistance [kN]
$f_u$	=	Ultimate tensile strength [N/mm <sup>2</sup> ]
$h_{net,d}$	=	Design value of the net heat flux per unit area (determined with EN 1991-1-2);
$I$	=	Second moment of area [mm <sup>4</sup> ]
$k$	=	Spring stiffness
$k_{sh}$	=	Correction factor for the so-called shadow effect;
$L$	=	Length [mm]
$L_{buc}$	=	Buckling length [mm]
$n$	=	Hardening factor of the Ramberg Osgood relationship
$t$	=	Plate thickness [mm]

#### Subscripts

$al$	=	aluminium
$g$	=	gas
$r$	=	radiation
$p$	=	protection material
$fi$	=	fire
$\theta$	=	property at temperature $\theta_{al}$
$inel$	=	inelastic
$cr$	=	critical

## References

- [1] Gale W.F., Totemeier, T.C. (2003) *Smithells Metals Reference Book*, 8th ed. Elsevier Butterworth-Heinemann, Amsterdam
- [2] Cadorin, J.F., Pintea, D. and Franssen, J.M. (2004) "The design fire tool ozone V2.0 – Theoretical description and validation on experimental fire tests", 1st draft, Université de Liège, département M&S, Rapport interne SPEC/2001-01
- [3] Dorn, J.E. (1954) "Some fundamental experiments on high temperature creep", *Journal of the mechanics and physics of solids*, Vol. 3, pp. 85-116
- [4] Dotreppe, J.C.; Hahn, C.; Haseltine, B.A.; Kersken-Bradley, M.; Krampf, L.; Kruppa, J.; Law, M.; Mathez, J.; Pedersen, E.; Schaumann, P.; Schleich, J.B.; Storti, G. and Twilt, L. (1990) "Actions on structures exposed to fire", Commission of European Communities, Eurocodes Chapter 20
- [5] EN 1993-1-2 (2005) "Eurocode 3: Design of steel structures – Part 1-2: General Rules – Structural fire design"
- [6] EN 1999-1-2 (2007) "Eurocode 9: Design of aluminium structures – Part 1-2: General Rules – Structural fire design"
- [7] Franssen, J.M. and Zaharia, R. (2006) "Design of steel structures subjected to fire – background and design guide to Eurocode 3", 2nd ed. University of Liege, Liege
- [8] Harmathy, T.Z. (1967a) "Deflection and failure of steel-supported floors and beams in fire, Symposium on fire test methods-restraint & smoke" 1966 ASTM STP 422, Am. Soc. Testing Mats., pp. 40-62
- [9] Harmathy, T.Z. (1967b) "A comprehensive creep model", *Journal of basic engineering*, Vol. 89, pp. 496-502
- [10] Holman, J.P. (2010) *Heat Transfer*, McGraw-Hill Higher Education, Boston
- [11] Kammer, C. (2002) *Aluminium Taschenbuch 1. Grundlagen und Werkstoffe*, 16th ed. Aluminium Verlag, Düsseldorf
- [12] Kaufman, J.G. (1999) "Properties of aluminium alloys – Tensile, creep and fatigue data at high and low temperatures", ASM international, Metals Park
- [13] Kruppa, J. (1996) "Performance-based code in fire resistance: first attempt by Eurocodes", in: *Proc. of International conference on performance-based codes and fire safety design method*, Ottawa
- [14] Kruppa, J.; Joyeux, D.; Zhao, B. (2005) "Scientific background to the harmonization of structural Eurocodes", *Heron*, Vol 50, pp. 219-236

- [15] Langhelle, N.K. (1999) "Experimental validation and calibration of nonlinear finite element models for use in design of aluminium structures exposed to fire", Ph.D. thesis, Norwegian University of Science and Technology, Trondheim
- [16] Langhelle, N.K., Eberg, E., Amdahl, J. and Lundberg, S. (1996) "Buckling tests of aluminium columns at elevated temperatures", in: *Proc. of 15th OMAE*, Firenze
- [17] Maljaars, J. and Soetens, F. (2006) "Brandwerendheid aluminium constructies – Eindrapport fase A" (in Dutch), TNO report 2006-D-R1062, TNO, Delft
- [18] Maljaars, J. Soetens, F. and Twilt, L. (2006) "Heating of aluminium members exposed to natural fire conditions", in: *Proc. of SIF '06*, Aveiro, pp. 75-88
- [19] Maljaars, J. (2008) "Local buckling of slender aluminium sections exposed to fire", Ph.D. thesis, Eindhoven University of Technology, Eindhoven
- [20] Maljaars, J., Soetens, F. and Katgerman, L. (2008) "Constitutive model for Aluminum Alloys Exposed to Fire Conditions", *Metallurgical and Materials Transactions A*, Vol. 39, pp. 778-789
- [21] Maljaars, J. and Soetens, F. (2009a) "Brandwerendheid aluminium constructies – Experimenteel en numeriek onderzoek naar aluminium portalen" (in Dutch), TNO report 034-DTM-2009-03417 and TNO report 034-DTM-2009-03180, TNO, Delft
- [22] Maljaars, J. and Soetens, F. (2009b) "Strength of MIG welded connections in fire exposed aluminium structures", *Journal of Advanced Steel Construction*, Vol. 5, pp. 136-150
- [23] Maljaars, J. Twilt, L. and Soetens, F. (2009c) "Flexural buckling of fire exposed aluminium columns", *Fire Safety Journal*, Vol. 44, pp. 711-717
- [24] Maljaars, J., Soetens, F. and Snijder, H.H. (2009d) "Local buckling of aluminium structures exposed to fire. Part 1: tests", *Thin Walled Structures*, Vol. 47, pp.1404-1417
- [25] Maljaars, J., Soetens, F. and Snijder, H.H. (2009e) "Local buckling of aluminium structures exposed to fire. Part 2: finite element models", *Thin Walled Structures*, Vol. 47, pp.1418-1428
- [26] Maljaars, J., Soetens, F. and Snijder, H.H. (2010) "Local Buckling of Fire-Exposed Aluminum Members – A New Design Model", *Journal of Structural Engineering*, Vol. 136, pp. 66-75
- [27] Van der Meulen, O. R. (2009) "Literature study on Collapse mechanisms of aluminium structures in fire", Eindhoven University of Technology, Eindhoven
- [28] Shanley, F.R. (1947) "Inelastic column theory", *Journal of the aeronautical sciences*, Vol. 14, pp. 261-268

- [29]Stowell, E.Z. (1948) "A unified theory of plastic buckling of columns and plates", Technical report no. 1556, National advisory committee for aeronautics, Washington D.C.
- [30]Twilt, L. and Van Oerle, N.J. (1999) "Natuurlijk brandconcept" (SG/TC3) (in Dutch), in: *Proc. of SG Techniekdag*, Delft
- [31]Twilt, L. (1991) "Global investigation into the resultant emissivity of aluminium alloys", CEN/TC 250/SC 9/PT 4/N 70.
- [32]Twilt, L.; Cajot, L.G.; Joyeux, D.; Van de Leur, P.; Kruppa, J.; Schleich, J.B. (1996) "Input data for natural fire design of building structures", in: *Proc. of IABSE colloquium*, Delft
- [33]Wang, Z.-H. and Tan, K.H. (2006) "Sensitivity study of time delay coefficient of heat transfer formulations for insulated steel members exposed to fire", *Fire safety Journal*, Vol. 41, pp. 31-38
- [34]De Witte, F.C. and Kikstra (2007) W.P. "DIANA users manual" - release 9.2, TNO Diana, Delft
- [35]Witteveen, J. and Twilt, L. (1975) "Behaviour of steel columns under fire action", in: *Proc. of IABSE*, Zürich, pp. 162-170